Applied Physics A (2020) 126:638
https://doi.org/10.1007/s00339-020-03827-5

Applied Physics A
Materials Science & Processing

Study of the photocatalytic activity of irradiated WO_3 microparticles

Artem L. Kozlovskiy[1,2,3] · **Maxim V. Zdorovets**[1,2,4]

Received: 21 May 2020 / Accepted: 20 July 2020 / Published online: 23 July 2020

Abstract
The work is devoted to the study of the effect of irradiation of commercial WO_3 microparticles with low-energy helium ions on the structural properties and photocatalytic activity during the decomposition of organic dyes. The irradiation fluences of 1×10^{13}–10^{15} ion/cm^2 were selected so that the number of defect overlap areas corresponded from 10 to 1000, but helium inclusions were not formed. It was found that with an increase in the radiation dose to 1015 ion/cm^2, partial degradation of the structural properties of microparticles is observed due to destruction of the surface layer and subsequent amorphization. Photocatalytic tests showed that for the initial microparticles not exposed to irradiation, the degree of decomposition of the indigo carmine dye was no more than 45–50% after 300 min, while for irradiated microparticles with a fluence of 10^{13} ion/cm^2, complete decomposition was observed after 200 min, and for microparticles irradiated 10^{14} ion/cm^2, complete dye decomposition is observed after 270 min. Partial amorphization upon irradiation with 10^{15} ion/cm^2 leads to a decrease in the degree of decomposition and a decrease in photocatalytic activity. In the case of decomposition of the congo red dye, the initial microparticles amounted to no more than 20% of the initial composition. For modified microparticles, an increase in the degree of decomposition is observed up to 45–50%.

Keywords Microparticles · Photocatalysis · Radiation defects · Structural changes · Helium ions

1 Introduction

In recent years, more and more attention has been paid to oxide or nitride micro- and nanostructured materials, as well as to various forms of their compounds, the interest in which is determined by their physicochemical, structural, strength and corrosion properties, which determine their huge application potential [1–3]. At the same time, the possibility of varying structural properties and morphology, as well as changing the specific surface area and particle size, opens up wide opportunities for researchers to use oxide micro- and nanostructures in solving technological problems, such as photocatalysis, microelectronics, wastewater treatment, solar energy [4–7]. Among the oxide compounds, tungsten oxide (WO_3) with a high melting point, good resistance to most aggressive media, and good catalytic properties for accelerating hydrocarbon cracking and hydrogeneration reactions is especially prominent [8–10]. Due to its redox potential, tungsten oxide has found its application as the basis of photocatalysts for the decomposition of organic dyes and pollutants [10–12].

For instance, a research group led by Martinez D. [1–3,6] conducted a series of experiments aimed at studying the photocatalytic activity of nano- and WO_3 microparticles in the decomposition of organic dyes. In the course of these studies, size dependence of the increase in photocatalytic activity was established, as a result of which it was determined that the smaller the grain size and the larger the active surface area, the higher the photoactivity and reaction rate [1–3,6].

However, despite all the advantages of these structures compared to other photocatalysts, such as titanium oxide, zinc oxide, etc., the problem of increasing photoactivity is one of the most relevant today, the solution of which will

✉ Artem L. Kozlovskiy
kozlovskiy.a@inp.kz

Maxim V. Zdorovets
mzdorovets@inp.kz

[1] Engineering Profile Laboratory, L.N. Gumilyov, Eurasian National University, Nur-Sultan 010008, Kazakhstan

[2] Laboratory of Solid State Physics, The Institute of Nuclear Physics, Almaty 050032, Kazakhstan

[3] Laboratory of Additive Technologies, Kazakh-Russian International University, Aktobe 030006, Kazakhstan

[4] Department of Intelligent Information Technologies, Ural Federal University, 620075 Yekaterinburg, Russia

significantly reduce the energy consumption and cost of the catalysts. The most common way to increase photoactivity is to modify the properties of microparticles by producing composites, such as $CuBi_2O_4/WO_3$ and CuO/WO_3, which are highly effective for the decomposition of dyes when exposed to visible light [13–15]. However, obtaining such composites is associated with high technological costs, which are not always cost-effective.

So, one of the ways to increase photoactivity is to modify properties by changing the crystal structure, as well as the specific surface area, which plays one of the fundamental roles in photocatalysis [11,16–18]. In view of the high radiation resistance of WO_3 microparticles, the use of ionizing radiation with doses characteristic of structural transformations arising in the case of the effect of overlapping defective regions (10^{13}–10^{15} ion/cm^2) can be used for directional modification of structural properties. At the same time, the use of low-energy ion beams with high doses or high densities has proven itself as methods of modifying and hardening materials [19,20], changing the optical properties of crystals [21–24], changing the phase composition of materials [25,26], and increasing the stability of materials corrosion and degradation [27,28].

Based on the foregoing, the aim of this research work is to assess the prospects of using low-energy irradiation with helium ions, which have a large ionizing ability, to change the structural and morphological features and increase the photocatalytic properties of WO_3 microparticles. The novelty of this scientific research lies in the search for optimal conditions for the modification of microstructures to increase the efficiency of their use. The obtained data on the effect of ionizing radiation will subsequently and significantly expand the field of application of ion beams in modern materials science.

2 Experimental part

2.1 Object of study

WO_3 microparticles, manufactured by Sigma Aldrich (chemical purity–99.9%, particle size ≤ 3 μm), with a monoclinic-type crystal structure and spatial syngony P21/n (14) were selected as initial objects. The choice of these microparticles as objects of study is due to their commercial availability, as well as high resistance to high-dose irradiation [29].

2.2 Modification of structural properties

Irradiation with low-energy helium ions (He^{2+}) with an energy of 40 keV was carried out at the DC-60 heavy ion accelerator (Nur-Sultan, Kazakhstan). Irradiation fluences of 1×10^{13}–10^{15} ion/cm^2 were selected so that the number of defect overlap areas corresponded from 10 to 1000, but helium inclusions did not form, causing material degradation and a decrease in strength properties [29,30]. The maximum mean free path of He^{2+} ions was 230–250 nm; the number of vacancies formed by one ion was 55 vacancies/ion. This depth of ion penetration corresponds to the surface layer, which plays a major role in the absorption properties of the material. Earlier in [29], we studied the kinetics of radiation damage in WO_3 microparticles, according to which it was found that radiation doses of—10^{15} ion/cm^2 are most optimal for structural modifications of microparticles without significant radiation damage that can lead to a sharp increase in the degree of amorphization of the structure.

2.3 Study of structural and morphological features

The morphology of the surface layer of microparticles was studied using scanning electron microscopy ("Hitachi TM4000" scanning electron microscope [Hitachi Ltd., Chiyoda, Tokyo, Japan)] and transmission electron microscopy (TEM microscope JEM 2100 LaB_6 or ARM200F, JEOL, Ltd., Tokyo, Japan). Changes in structural parameters and dislocation density were carried out by evaluating X-ray diffraction patterns obtained in the Breg–Brentano geometry at $2\theta = 20$–$50°$, in increments of $2\theta = 0.01°$ [D8 Advance Eco powder diffractometer (Bruker, Karlsruhe, Germany)]. To decrypt and analyze the obtained diffraction patterns, the DiffracEva 4.2 software was used.

The band gap measurements were obtained by measuring the UV–Vis spectra on a Jena Specord-250 BU analytical spectrophotometer.

2.4 Photocatalytic activity tests

The photocatalytic properties of WO_3 microparticles before and after modification were evaluated by decomposition of organic dyes indigo carmine (IC) and congo red (CR) in water. A box made of borosilicate glass immersed in water to maintain room temperature during processing with a xenon lamp (2100 lm) was used as a photochemical reactor. The concentration of WO_3 microparticles was 10 mg/L. Initial dye concentrations were 30 mg/L for IC and 20 mg/L for CR. The test interval was 300 min in increments of 30 min, the pH of the solution was 5.2, the stirring speed was 100 rpm, and intensive stirring was necessary to prevent the accumulation of sediment in two boxes as a result of conglomeration of microparticles.

3 Results and discussion

Figure 1 shows TEM images of WO_3 microparticles before and after irradiation with He^{2+} ions.

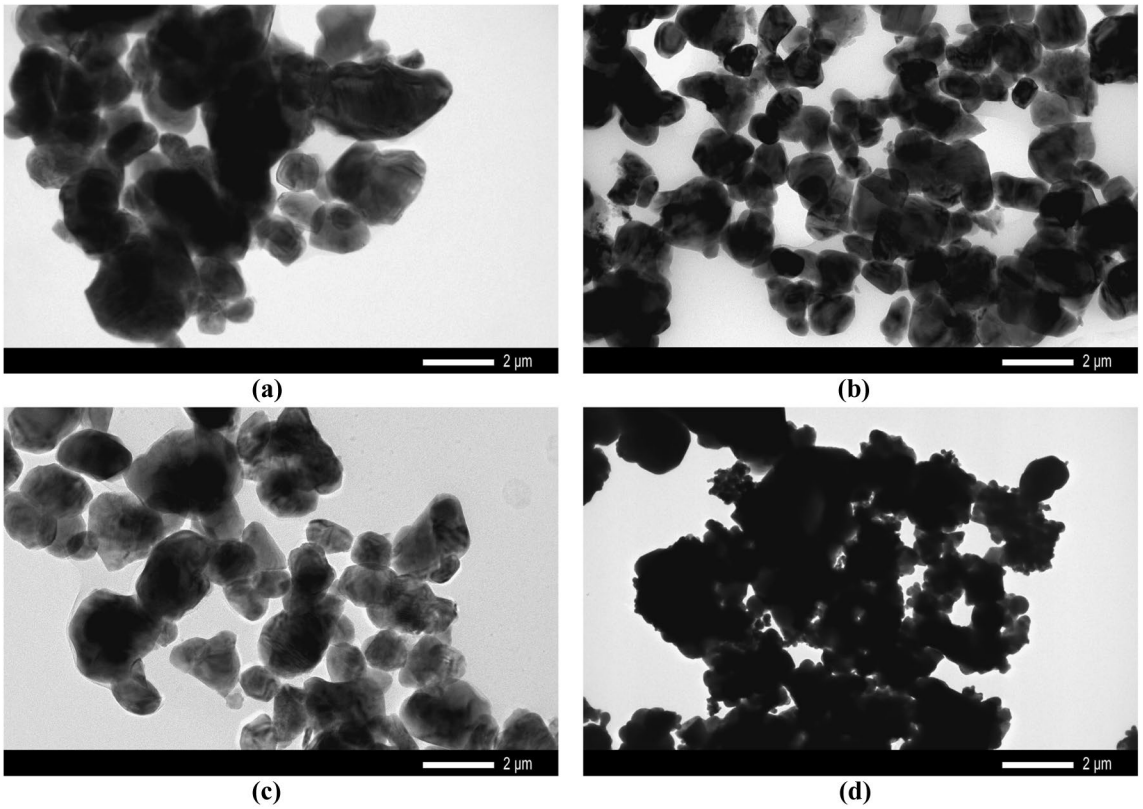

Fig. 1 TEM images of the studied WO_3 microparticles before and after irradiation: (**a**) Initial sample; (**b**) 10^{13} ion/cm^2; (c) 10^{14} ion/cm^2; (**d**) 10^{15} ion/cm^2

The greatest morphological changes are observed for samples irradiated with doses of 10^{14}–10^{15} ion/cm^2 at which structural changes in the surface layer are most affected by ion irradiation. At the same time, at an irradiation dose of 10^{15} ion/cm^2, a partial amorphization of the surface layer is observed, which is clearly visible on the SEM image of the surface of the microparticles shown in (Fig. 2). The degradation of the surface layer is due to the fact that an increase in the radiation dose leads to an increase in the density of cascade defects in the structure due to the effect of overlapping defective areas. Moreover, for low-energy particles, the energy losses in the case of collisions with electron shells

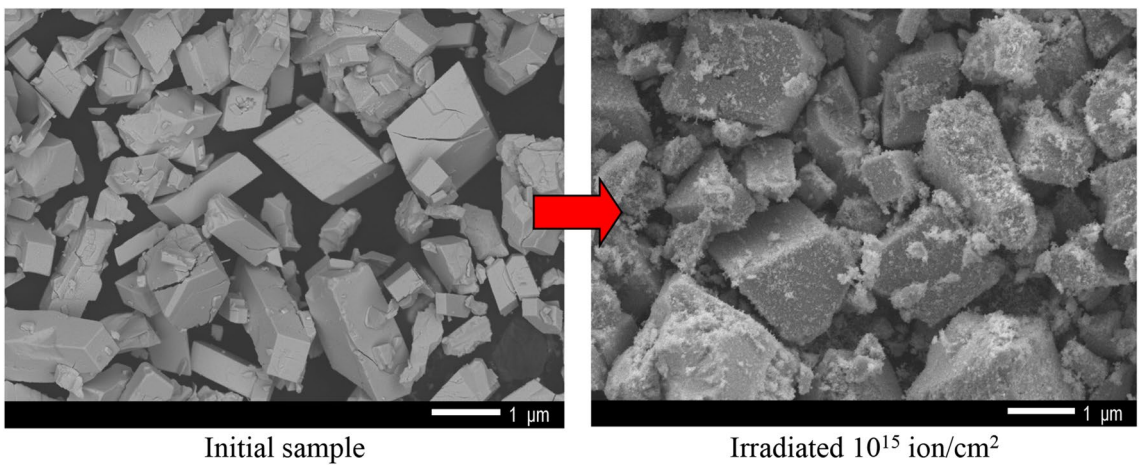

Fig. 2 SEM images of changes in the structure of WO_3 microparticles after irradiation with a dose of 10^{15} ion/cm^2

and target nuclei are equal, and in some cases, nuclear losses prevail, which lead to the formation of a large number of initially knocked-out atoms. Due to the difference in atomic radii, as well as the binding energy of tungsten and oxygen, as well as due to the low solubility of helium ions and the high probability of their agglomeration in the case of high doses, the surface layer undergoes a large destructive effect, leading to partial amorphization and degradation of the structure. In the case of small doses of radiation, the effect of accumulation of defects is much lower, and irradiation can lead to partial reorientation or recrystallization of grains due to the transferred energy from incident ions, which leads to not so destructive consequences.

Figure 3 shows the results of changes in X-ray diffraction patterns of the studied WO_3 microparticles before and after irradiation, as well as detailed representations of the changes in the three main diffraction maxima characterizing the structural changes in the crystal lattice of the monoclinic type. Table 1 presents the data on the changes in the basic crystallographic characteristics of WO_3 microparticles before and after irradiation.

According to the data presented, the main changes in X-ray diffraction patterns at low radiation doses of 10^{13}–10^{14} ion/cm^2 are associated with a decrease in the intensity of diffraction maxima, which is caused by a change in the orientation position of crystallites in the structure of microparticles, as well as a shift of diffraction maxima to the region of small angles, which indicates an increase in the strain and distortions of the crystal structure due to irradiation. However, an increase in the irradiation fluence to 10^{15} ion/cm^2 leads to the formation of a halo, which confirms the previously observed data

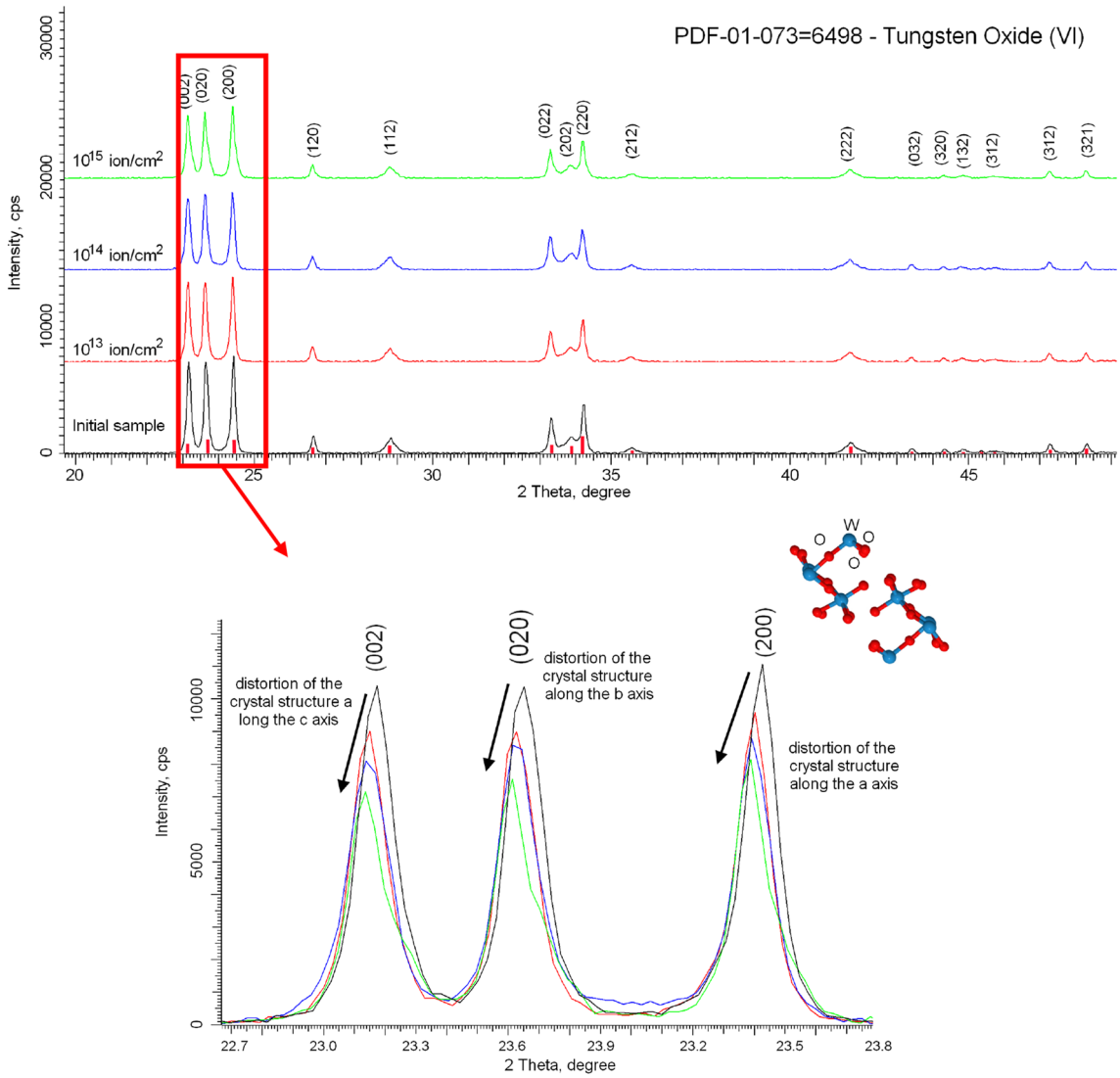

Fig. 3 X-ray diffraction patterns of the investigated WO_3 microparticles before and after irradiation

Table 1 Structural data for WO_3 microparticles

Structural parameter	Initial sample	1×10^{13} ion/cm^2	1×10^{14} ion/cm^2	1×10^{15} ion/cm^2
Lattice parameter, Å	$a=7.2845$	$a=7.2903$	$a=7.2932$	$a=7.2961$
	$b=7.5176$	$b=7.5236$	$b=7.5266$	$b=7.5296$
	$c=7.6705$	$c=7.6797$	$c=7.6829$	$c=7.6858$
	$\beta=90.91$	$\beta=90.97$	$\beta=91.01$	$\beta=91.5$
Volume unit cell, Å^3	420.0	421.16	421.66	422.17
Crystalline size, nm	73.1 ± 4.2	70.7 ± 2.1	64.5 ± 2.3	57.4 ± 4.1
Density, g/cm^2	7.330	7.311	7.303	7.294
Specific surface area, m^2/g	0.011	0.116	0.0127	0.0142
Integral porosity, %	0.13	0.25	0.36	0.49
The degree of perfection of the crystal structure, (%)	85.6	84.4	83.2	75.8
BET surface area (m^2 g^{-1})	11.19	11.61	12.74	14.33

on the amorphization and degradation of microparticles. It is also worth noting that the decrease in the intensities and the shift of the diffraction maxima (002), (020) and (200), which reflect the deformation of the crystal lattice along the crystallographic axes, are almost the same as the decrease in the intensities, which indicates that the deformation of the lattice occurs along all axes of the crystal are equally probable. Moreover, according to the data obtained, the largest change in structural parameters, in particular, an increase in porosity and a decrease in density, is observed for samples irradiated with a maximum radiation dose. Also, an increase in the radiation dose leads to initialization of the processes of recrystallization and crushing of crystallites, as evidenced by a decrease in grain sizes, as well as an increase in the specific surface area, which can significantly affect the photocatalytic ability of the selected microparticles.

Table 1 presents the results of changes in the specific surface area (BET surface area) of microparticles depending on the radiation dose. As can be seen from the presented data, an increase in the radiation dose leads to a slight increase at a radiation dose of 10^{13} ion/cm^2 by 3.7%, while an increase in the radiation dose to 10^{14} and 10^{15} ion/cm^2 leads to an increase in BET surface area by 13.8% and 28.1%, respectively.

Figure 4 shows the results of the transmission spectrum processing and Tauc's plot construction, which were obtained to determine the magnitude of the band gap (E_g). According to the calculated data for the initial microparticles, the value of $E_g=2.77$ eV, while for irradiated samples, there is a tendency to decrease this value depending on the radiation dose.

The study of the photocatalytic activity of WO_3 microparticles before and after irradiation was carried out by assessing the decomposition of the organic dyes indigo carmine and congo red in an aqueous solution when exposed to visible light. Figures 5 and 6 show the dynamics of changes in

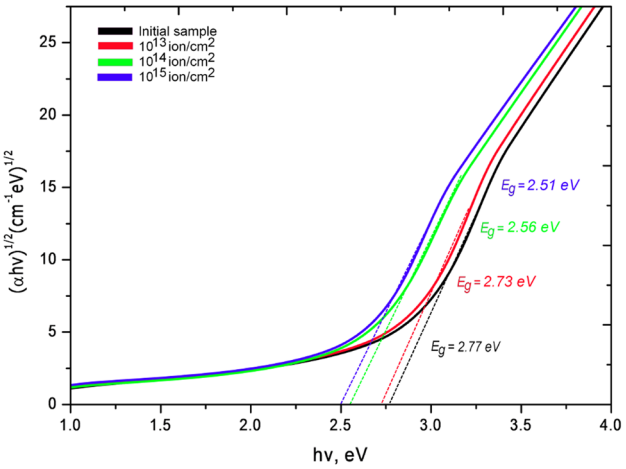

Fig. 4 Tauc's plot

the UV absorption spectra of indigo carmine and congo red depending on the type of catalysts.

Figure 7 shows the time dependence of photocatalytic degradation, which was estimated by comparing the concentration of the dye in the solution before and after a given time interval. As a comparative characteristic, a graph of the photocatalytic degradation of a dye without the addition of microparticles is presented, which shows the absence of any changes in the dye concentration in a solution over time without the addition of catalysts.

In the case of the initial microparticles, the degree of photocatalytic decomposition of the indigo carmine dye was no more than 45–50% after 300 min of testing under the influence of light, and the degradation rate decreased after 150 min. For irradiated structures, an increase in the degree of decomposition of dyes is observed; in the case of the indigo carmine dye, for samples irradiated with a fluence of 10^{13} ion/cm^2, complete decomposition is observed after 200 min, and for microparticles irradiated with 10^{14} ion/

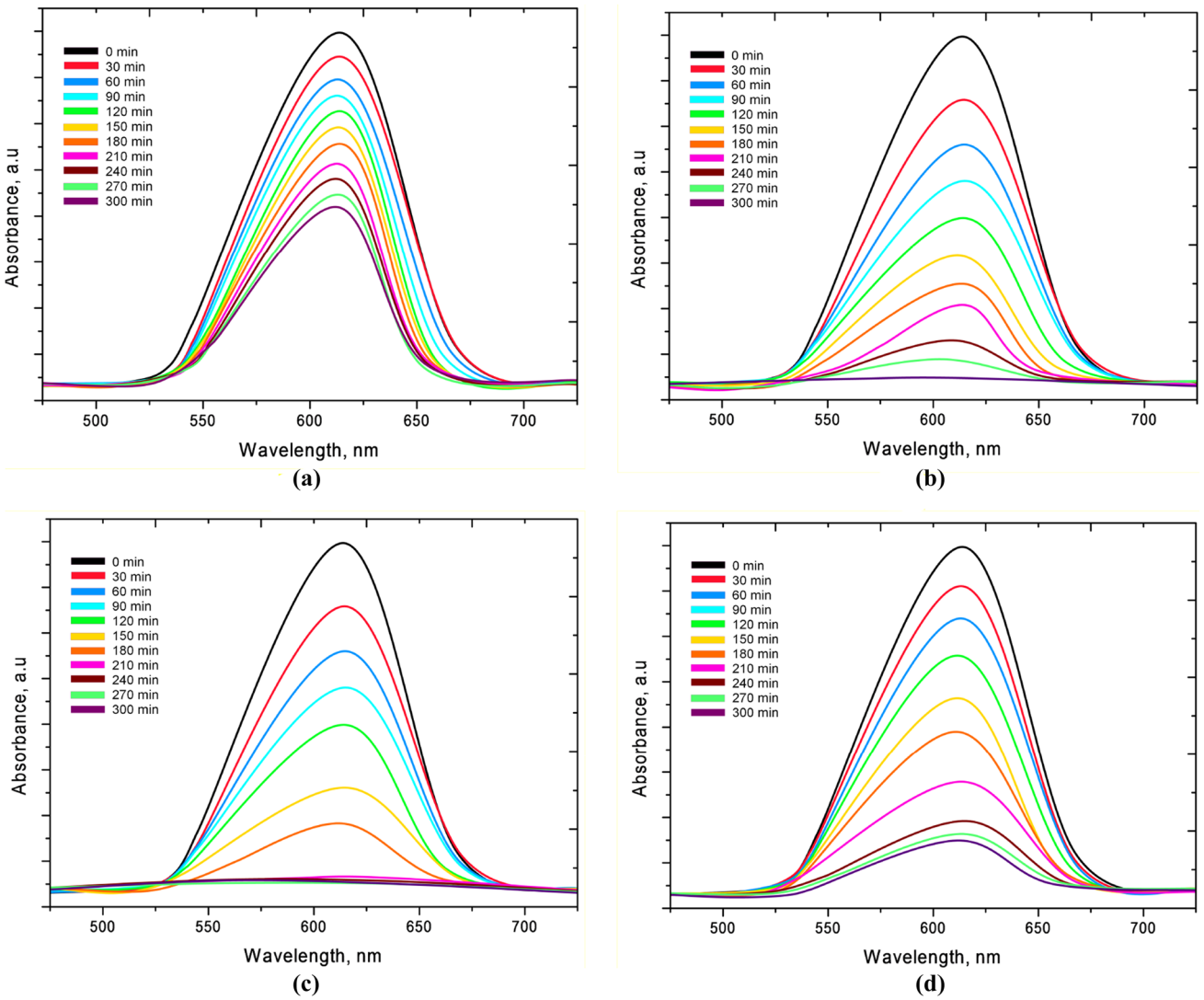

Fig. 5 Dynamics of changes in the UV absorption spectra of indigo carmine depending on the type of catalysts: (**a**) initial sample; (**b**) 10^{13} ion/cm^2; (**c**) 10^{14} ion/cm^2; (**d**) 10^{15} ion/cm^2

cm^2, complete decomposition of the dye is observed after 270 min. However, an increase in the irradiation fluence to 10^{15} ion/cm^2 leads to a decrease in the degree of decomposition of indigo carmine, which may be due to a deterioration in the crystalline properties of microparticles, as well as the formation of disorder regions in the structure of the surface layer, which reduces the activity of decomposition.

For the initial microparticles, the degree of decomposition of the congo red dye was no more than 20%. For modified microparticles, an increase in the degree of decomposition is observed up to 45–50%; however, as in the case of the indigo carmine dye, an increase in the irradiation fluence to 10^{15} ion/cm^2 leads to a decrease in the degree of decolorization of the solution. The low degree of decomposition of congo red is due to the presence of an azo (-N=N-) group in the structure of the dye, which has a high binding energy, which requires more energy or an increase in the concentration of the catalyst to break.

Figure 8 shows the results of photocatalytic activity in the case of a twofold increase in catalyst concentration for both dye decomposition reactions.

As can be seen from the data presented, an increase in the concentration in the case of the decomposition reaction of the indigo carmine dye led to an increase in the decomposition rate and to achieve the maximum degree of dye discoloration within 150 min and 180 for samples irradiated with doses of 10^{13} ion/cm^2 and 10^{14} ion/cm^2, respectively. Moreover, complete dye decomposition is also observed for

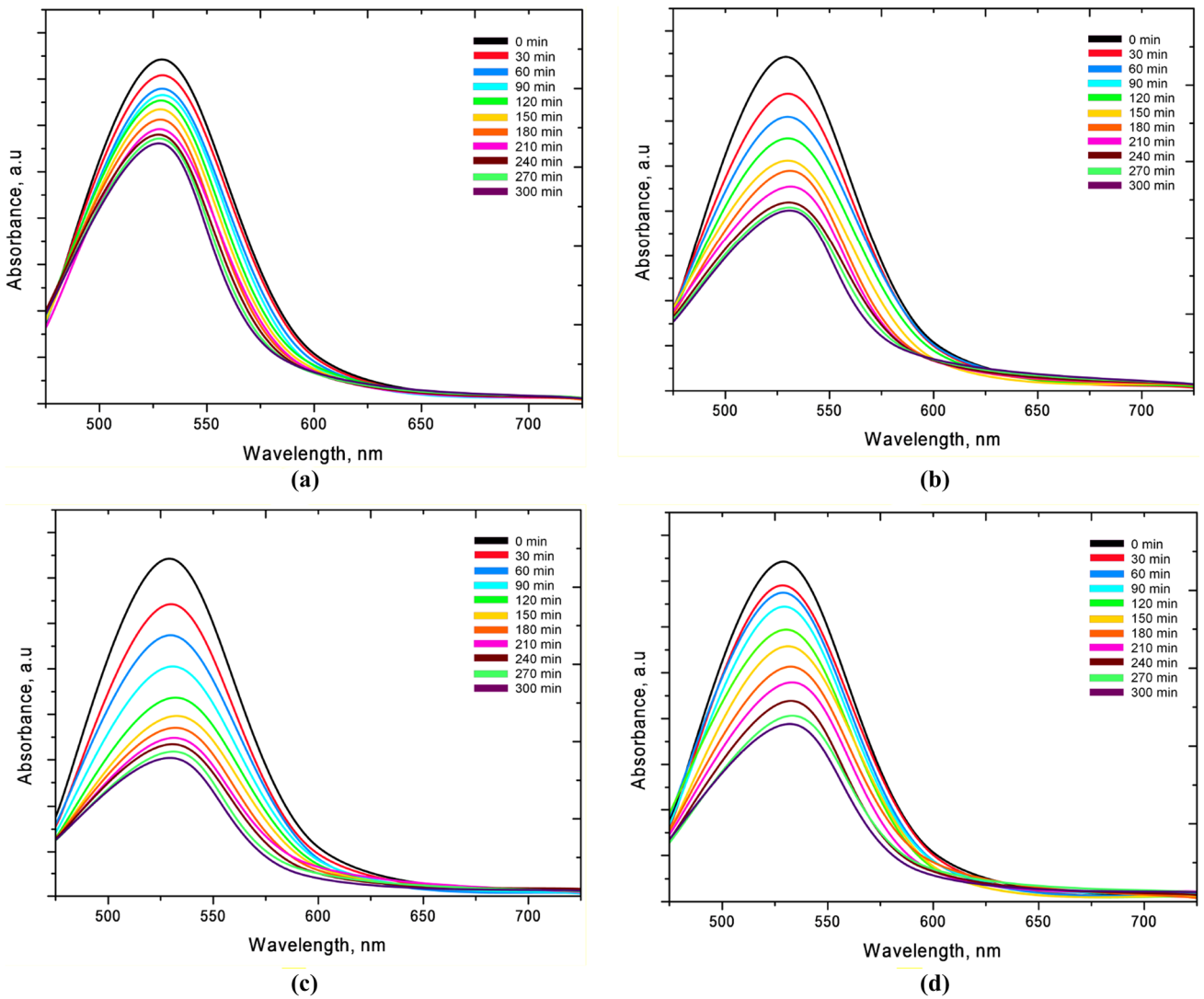

Fig. 6 Dynamics of changes in the UV absorption spectra of congo red depending on the type of catalysts: (**a**) initial sample; (**b**) 10^{13} ion/cm^2; (**c**) 10^{14} ion/cm^2; (**d**) 10^{15} ion/cm^2

samples irradiated with a dose of 10^{15} ion/cm^2 after 240 min. In the case of the congo red decomposition reaction, an increase in the dye concentration leads to a slight increase in the decomposition rate, as well as a decrease in the dye concentration in the solution to 40% for irradiated samples. A small decrease in the concentration of congo red dye in the case of an increase in the concentration of the catalyst indicates the lack of efficiency of increasing the proportion of catalyst in the solution to increase the degree of decomposition. However, in the case of indigo carmine decomposition, an increase in the catalyst fraction by a factor of two leads to a significant reduction in energy consumption during the industrial scale photocatalytic decomposition of dyes.

Figure 9 shows the results of evaluating the degree of mineralization depending on the type of photocatalyst, which was evaluated by determining the change in the concentration of total organic carbon (TOC) after the end of the cycle of the photocatalytic decomposition reaction. According to the data presented, the highest degree of mineralization (more than 40%, for IC and 29% CR) is for samples irradiated with a dose of 10^{14} ion/cm^2, for which complete discoloration of the solution is observed for 210 min in the case of photodegradation of the IC dye. A low degree of mineralization of solutions, even in the case of complete discoloration of solutions, may be due to the processes of inactivation of chromospheric groups in the dye, as well as

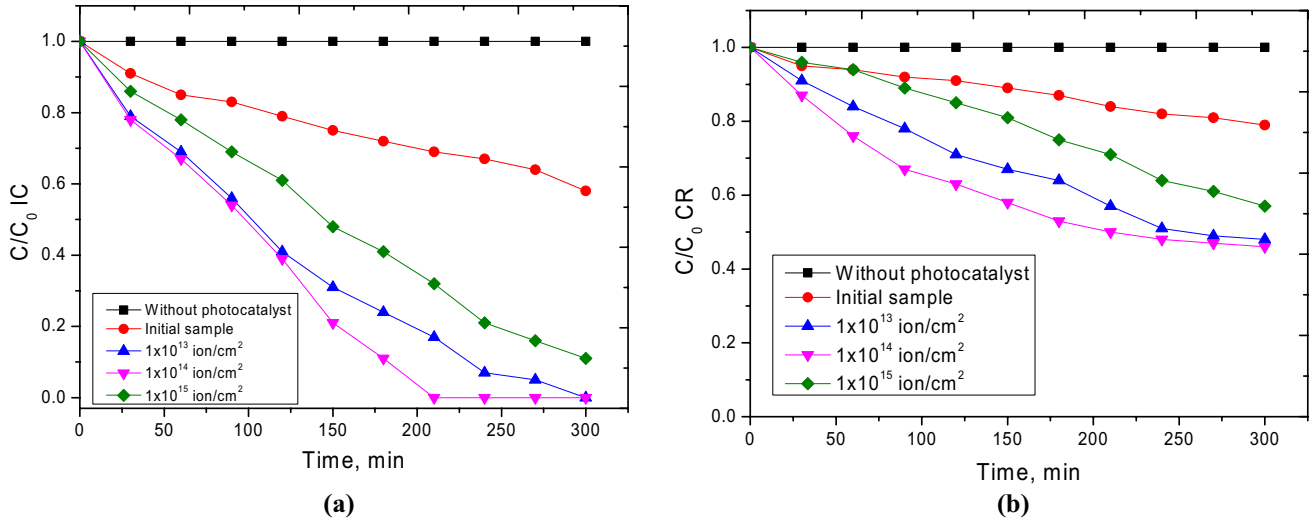

Fig. 7 The dynamics of the curve of photocatalytic degradation of organic dyes: (**a**) IC; (**b**) CR

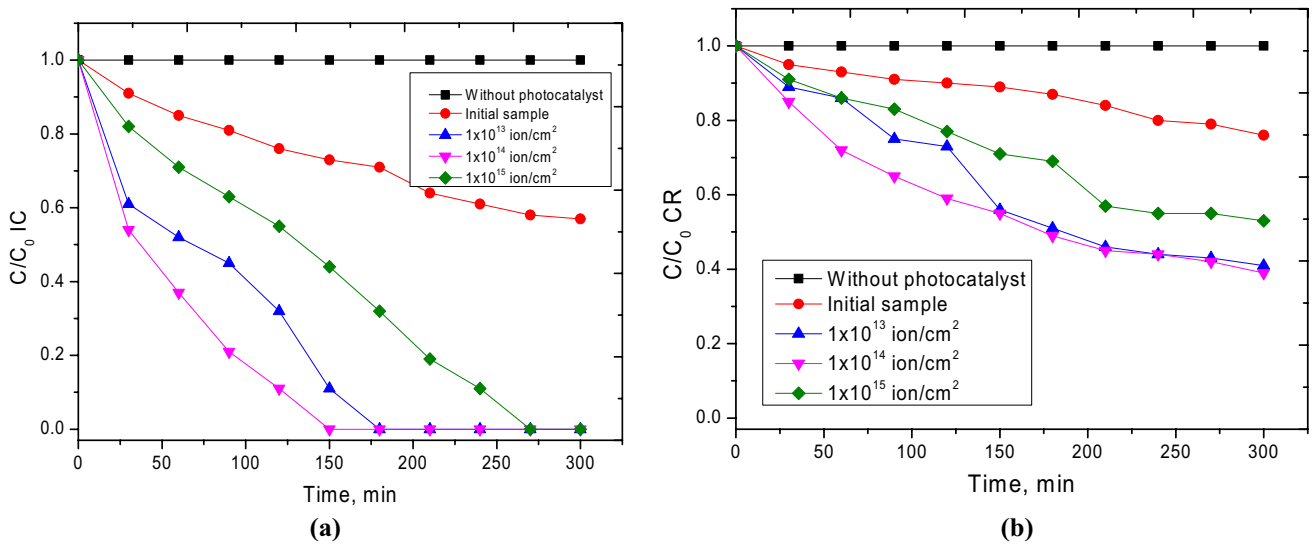

Fig. 8 The dynamics of the curve of photocatalytic degradation of organic dyes with an increase in the concentration of the catalyst in 2 times: (**a**) IC; (**b**) CR

partial adsorption of the dye on the surface of microparticles [31].

One of the important characteristics of the catalysts is the preservation of the operability and efficiency of decomposition for not only a long time, but also the number of cycles, which is one of the important factors in assessing the prospects of photocatalysts. Figure 10 shows a graph of the degree of photocatalytic decomposition of indigo carmine and congo red dyes after 300 min of testing for ten cycles of sequential tests.

From the presented diagram, it is seen that the degree of decomposition of the dyes remains almost constant for irradiated samples for 5–7 cycles, while for the initial microparticles, the degree of decomposition decreases after four test cycles. Moreover, the decrease in the degree of decomposition for the irradiated samples is much less than for the

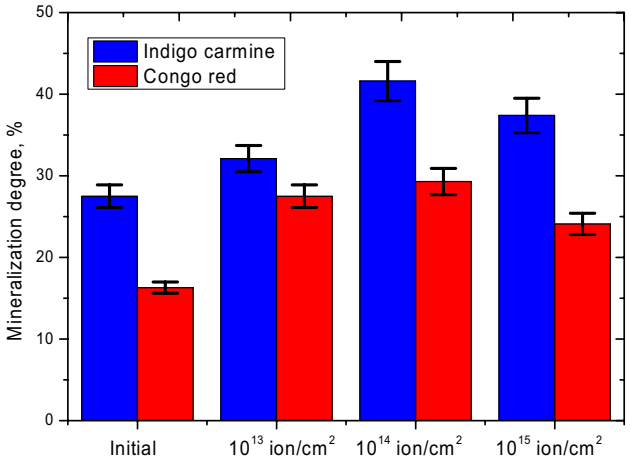

Fig. 9 Diagram of changes in the degree of mineralization depending on the type of photocatalyst

initial microparticles, which indicates the long-term effect of maintaining the photocatalytic ability of the irradiated microparticles.

Today, one of the most promising areas for the practical use of both microparticles and thin films is photocatalysis and the decomposition reaction of various harmful substances and dyes. Moreover, interest in nanostructured and microstructural objects compared to massive objects of a similar composition is due to the fact that, due to the small size, their properties have significant differences, as well as a relatively large specific surface area. So, for example, (Table 2) presents comparative data of recent studies in the field of application of microstructures and thin films in photocatalysis.

Thus, even a brief review of the literature data shows the promise of using various oxide micro- and nanostructures, as well as thin films as various photocatalysts.

4 Conclusion

The effect of irradiation of commercial WO_3 microparticles with low-energy helium ions on the structural properties and photocatalytic activity during the decomposition of organic dyes is considered. It was found that with an increase in the radiation dose to 10^{15} ion/cm^2, partial degradation of the structural properties of microparticles is observed due to destruction of the surface layer and subsequent amorphization. Photocatalytic tests showed that for the initial microparticles not exposed to irradiation, the degree of decomposition of the indigo carmine dye was no more than 45–50% after 300 min, while for irradiated microparticles with a fluence of 10^{13} ion/cm^2, complete decomposition was observed after 200 min, and for microparticles irradiated 10^{14} ion/cm^2, complete dye decomposition is observed after 270 min. Partial amorphization upon irradiation with 10^{15} ion/cm^2 leads to a decrease in the degree of decomposition and a decrease in photocatalytic activity. In the case of decomposition of the congo red dye, the initial microparticles amounted to no more than 20% of the initial composition. For modified microparticles, an increase in the degree of decomposition is observed up to 45–50%.

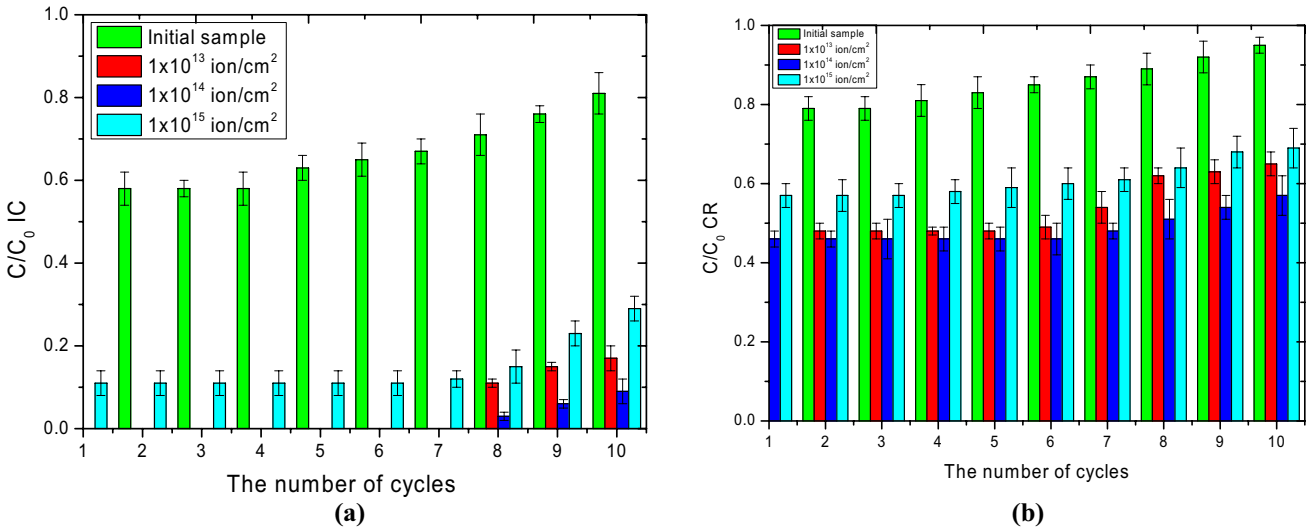

Fig. 10 Photocatalytic decomposition diagram of indigo carmine (**a**) and congo red (**b**) dyes after 300 min of testing for 10 cycles of sequential testing

Table 2 Comparative data from recent research on photocatalyst applications

Catalyst type	Reaction type	Main results	Source
TiO_2 thin films	Cr(VI) photocatalytic reduction	In this paper the dependences of the influence of the thickness of thin films on the photocatalytic reduction rate, as well as the efficiency of the photocatalytic reaction, are established. The authors found that increasing the thickness of the films can significantly increase the reaction rate and achieve complete recovery in less than 300 min	[32]
WO_3 microparticles	Photocatalytic decomposition of Ethylene (C2H4)	The prospects of applying the effect of doping Fe^{3+} on changes in the photocatalytic activity of ethylene decomposition are shown. The dependences of an increase in photocatalytic activity, as well as an increase in the life of doped Fe^{3+} microparticles in comparison with the initial microparticles, were established	[33]
TiO_2/WO_3 composite fibers	Photocatalytic decomposition reactions of methyl orange	The authors examined the prospects for the use of TiO_2/WO_3 composite fibers for photocatalytic bleaching of methyl orange as a result of exposure to UV radiation and visible light. It was shown that with an increase in the content of ammonium metatungstate in the composite structure, the reaction rate increased in visible light; for composites containing 50% fiber, the highest decomposition activity was observed under UV irradiation	[34]
Au–TiO_2-loaded cubic g-C_3N_4 nanohybrids	Photocatalytic decomposition reactions of methyl orange	The authors found that the increase in the photocatalytic activity of the synthesized nanohybrids is due to the double effect of the catalytically active Au and TiO_2 nanoparticles. It has also been shown that synthesized nanohybrids can be used as amine gases detectors	[35]

Author contributions conceptualization, M.V.Z., and A.L.K.; methodology, A.L.K.; formal analysis, M.V.Z.; investigation, A.L.K. and M.V.Z.; resources, M.V.Z.; writing—original draft preparation, review and editing, M.V.Z. and A.L.K.; visualization, M.V.Z.; supervision, M.V.Z.

Funding This study was funded by the Ministry of Education and Science of the Republic of Kazakhstan (grant BR05235921).

Compliance with ethical standards

Conflicts of interest The authors declare that they have no known competing financial interests or personal relationships that could have appeared to influence the work reported in this paper.

References

1. D. Martinez, A.-D. Sanchez, E. La Cruz, L. Cuéllar, Photocatalytic properties of WO3 nanoparticles obtained by precipitation in presence of urea as complexing agent. Appl Catalysis A Gen **398**(1–2), 179–186 (2011)
2. D. Sánchez-Martínez, A. Martínez-De La Cruz, E. López-Cuéllar, Synthesis of WO3 nanoparticles by citric acid-assisted precipitation and evaluation of their photocatalytic properties. Mater Res Bull **48**(2), 691–697 (2013)
3. A.B.D. Nandiyanto et al., Identification of micro-mechanical characteristics of monoclinic tungsten trioxide microparticles by nanoindentation technique. Mater Phys Mech **42**(3), 323–329 (2019)
4. H.O. Tekin, M.I. Sayyed, S.A.M. Issa, Gamma radiation shielding properties of the hematite-serpentine concrete blended with WO3 and Bi2O3 micro and nano particles using MCNPX code. Radiat Phys Chem **150**, 95–100 (2018)
5. N.A. Shik, L. Gholamzadeh, X-ray shielding performance of the EPVC composites with micro-or nanoparticles of WO3, PbO or Bi2O3. Appl Radiat Isotopes **139**, 61–65 (2018)
6. A. Martínez-de la Cruz, D. Sánchez Martínez, E. López Cuéllar, Synthesis and characterization of WO3 nanoparticles prepared by the precipitation method: evaluation of photocatalytic activity under vis-irradiation. Sol State Sci **12**(1), 88–94 (2010)
7. D.B. Hernandez-Uresti et al., Characterization and photocatalytic properties of hexagonal and monoclinic WO3 prepared via microwave-assisted hydrothermal synthesis. Ceram Internat **40**(3), 4767–4775 (2014)
8. M. Karimi-Nazarabad, E.K. Goharshadi, Highly efficient photocatalytic and photoelectrocatalytic activity of solar light driven WO3/g-C3N4 nanocomposite. Sol Energy Mater Sol Cells **160**, 484–493 (2017)
9. S. Wang et al., Visible light-driven photodecomposition system: preparation and application of highly dispersed Pt-loaded WO3 microparticles. Micro Nano Lett **6**(4), 229–232 (2011)

10. M.B. Tahir, M. Sagir, N. Abas, Enhanced photocatalytic performance of CdO-WO3 composite for hydrogen production. Internat J Hydrogen Energy **44**(45), 24690–24697 (2019)
11. M.B. Tahir et al., WO 3 nanostructures-based photocatalyst approach towards degradation of RhB dye. J Inorg Mater **28**(3), 1107–1113 (2018)
12. V. Iliev et al., Enhancement of photocatalytic oxidation of oxalic acid by gold modified WO3/TiO2 photocatalysts under UV and visible light irradiation. J Mol Catal A Chem **327**(1-2), 51–57 (2010)
13. T. Arai et al., Efficient complete oxidation of acetaldehyde into CO2 over CuBi2O4/WO3 composite photocatalyst under visible and UV light irradiation. J Phys Chem C **111**(21), 7574–7577 (2007)
14. L. Wei et al., Preparation, characterisation of p–n heterojunction photocatalyst CuBi2O4/Bi2WO6 and its photocatalytic activities. J Exper Nanosci **6**(2), 102–120 (2011)
15. J. Su et al., Nanostructured WO3/BiVO4 heterojunction films for efficient photoelectrochemical water splitting. Nano lett **11**(5), 1928–1933 (2011)
16. A. Mohagheghian et al., Enhanced photocatalytic activity of Fe3O4-WO3-APTES for azo dye removal from aqueous solutions in the presence of visible irradiation. Part Sci Technol **37**(3), 358–370 (2019)
17. M.B. Tahir, H. Kiran, T. Iqbal, The detoxification of heavy metals from aqueous environment using nano-photocatalysis approach: a review. Environ Sci Pollution Res **26**(11), 10515–10528 (2019)
18. M.B. Tahir et al., Fabrication of heterogeneous photocatalysts for insight role of carbon nanofibre in hierarchical WO3/MoSe2 composite for enhanced photocatalytic hydrogen generation. Ceram Internat **45**(5), 5547–5552 (2019)
19. H. Gnaser et al., Surface modification of GaAs (110) by low-energy ion irradiation. Phys Rev B **52**(19), 14086 (1995)
20. S.S. Tinchev, Surface modification of diamond-like carbon films to graphene under low energy ion beam irradiation. Appl Surf Sci **258**(7), 2931–2934 (2012)
21. R.S. Averback et al., Defects in ion implanted and electron irradiated MgO and Al2O3. Radiat Eff Defects Sol **136**(1-4), 169–173 (1995)
22. A.I. Popov, E. Balanzat, F centre production in CsI and CsI–Tl crystals under Kr ion irradiation at 15 K. Nucl Instrum Methods Phys Res **166**, 545–549 (2000)
23. A. Lushchik et al., Influence of complex impurity centres on radiation damage in wide-gap metal oxides. Nucl Instrum Methods Phys Res Sect B **374**, 90–96 (2016)
24. E.A. Kotomin, V.N. Kuzovkov, A.I. Popov, The kinetics of defect aggregation and metal colloid formation in ionic solids under irradiation. Radiat Eff Defects Sol **155**(1-4), 113–125 (2001)
25. V. Chauhan, R. Kumar, Phase transformation and modifications in high-k ZrO2 nanocrystalline thin films by low energy Kr5+ ion beam irradiation. Mater Chem Phys **240**, 122127 (2020)
26. A.L. Stepanov, I.B. Khaibullin, Fabrication of metal nanoparticles in sapphire by low-energy ion implantation. Rev Adv Mater Sci **9**(2), 109–129 (2005)
27. X. Xiao, Yu Long, Nano-indentation of ion-irradiated nuclear structural materials: a review. Nucl Mater Energy **22**, 100721 (2020)
28. A. Kozlovskiy et al., Structure and corrosion properties of thin TiO2 films obtained by magnetron sputtering. Vacuum **164**, 224–232 (2019)
29. M.V. Zdorovets et al., Helium swelling in WO3 microcomposites. Ceram Int **46**(8A), 10521–10529 (2020)
30. M. Zdorovets et al., Defect formation in AlN after irradiation with He2+ ions. Ceram Int **45**(7), 8130–8137 (2019)
31. C. Flox et al., Electro-Fenton and photoelectro-Fenton degradation of indigo carmine in acidic aqueous medium. Appl Catalysis B Environ **67**(1–2), 93–104 (2006)
32. A. Kleiman et al., Photocatalytic activity of TiO2 films prepared by cathodic arc deposition: dependence on thickness and reuse of the photocatalysts. Surf Coat Technol **382**, 125154 (2020)
33. X. Liu et al., Synthesis of a WO 3 photocatalyst with high photocatalytic activity and stability using synergetic internal Fe 3+ doping and superficial Pt loading for ethylene degradation under visible-light irradiation. Catalysis Sci Technol **9**(3), 652–658 (2019)
34. V.O. Odhiambo et al., Synthesis of TiO2/WO3 composite nanofibers by a water-based electrospinning process and their application in photocatalysis. Nanomaterials **10**(5), 882 (2020)
35. R. Malik et al., Au–TiO2-loaded cubic g-C3N4 nanohybrids for photocatalytic and volatile organic amine sensing applications. ACS Appl Mater Inter **10**(40), 34087–34097 (2018)